SELECTED PERFORMANCE MEASUREMENTS OF THE F-15 ACTIVE AXISYMMETRIC THRUST-VECTORING NOZZLE

John S. Orme[*] and Robert L. Sims[†]
NASA Dryden Flight Research Center
Edwards, California

Abstract

Flight tests recently completed at the NASA Dryden Flight Research Center evaluated performance of a hydromechanically vectored axisymmetric nozzle onboard the F-15 ACTIVE. A flight-test technique whereby strain gages installed onto engine mounts provided for the direct measurement of thrust and vector forces has proven to be extremely valuable. Flow turning and thrust efficiency, as well as nozzle static pressure distributions were measured and analyzed. This report presents results from testing at an altitude of 30,000 ft and a speed of Mach 0.9. Flow turning and thrust efficiency were found to be significantly different than predicted, and moreover, varied substantially with power setting and pitch vector angle. Results of an in-flight comparison of the direct thrust measurement technique and an engine simulation fell within the expected uncertainty bands. Overall nozzle performance at this flight condition demonstrated the F100-PW-229 thrust-vectoring nozzles to be capable and efficient.

Nomenclature

Acronyms

ACTIVE   Advanced Control Technology for Integrated Vehicles

BBN   balanced beam nozzle

HARV   High Alpha Research Vehicle

MATV   multi-axis thrust vectoring

NASA   National Aeronautics and Space Administration

Pamb   ambient pressure, lbf/in^2

P/Y BBN   pitch/yaw balanced beam nozzle

P&W   Pratt & Whitney, West Palm Beach, Florida

VMS   vehicle management system computer

Symbols

F_g gross thrust, lbf

F_g^* modified gross thrust (includes nozzle drag), lbf

$F_{g_x}^*$ axial component of modified gross thrust, lbf

F_p pitch vector force, lbf

F_R resultant gross thrust, lbf

F_R^* modified resultant gross thrust, lbf

F_{R0}^* modified resultant gross thrust at nonvectored conditions, lbf

$p/pt7$ static pressure normalized to nozzle inlet total pressure, $pt7$, lbf/in^2

x/L nondimensional distance along the flap, percent

δ_f vector force angle, positive trailing edge down, deg

δ_m vector metal angle, positive trailing edge down, deg

Introduction

Because of the strong potential for improved vehicle performance, thrust-vectoring nozzles are being considered for current and future aircraft designs. A number of recent flight test programs have included thrust-vectoring nozzles to demonstrate these potential vehicle performance benefits.[1-5] For most of these studies, the ability of thrust vectoring to augment aircraft stability and control and to improve handling qualities has been the primary focus of research. However, in-flight nozzle performance has not been closely examined for production design nozzles.

Limited nozzle performance evaluation was attempted during the testing of the F-18 High Alpha Research Vehicle (HARV) including parameter estimation techniques and ground test. However, the flight control law design made separating the thrust vectoring from aerodynamic control effectiveness extremely difficult and introduced large uncertainties.[6,7] Similarly, because

aerodynamic control surfaces and thrust vectoring of the F-16 multi-axis thrust vectoring airplane (MATV) were designed to move in unison, it was impossible to isolate the effects of each.[5]

None of the aforementioned programs specifically evaluated vectoring nozzle performance or measured vectoring loads in-flight. Uniquely, the initial focus of the NASA Dryden Flight Research Center Advanced Control Technology for Integrated Vehicles (ACTIVE) program has been development of a production design axisymmetric thrust-vectoring nozzle.[8] To avoid the difficulties identifying nozzle performance encountered by the HARV and MATV testing, the ACTIVE system provided for separating the vectoring system from the flight control system. The control system design allowed the nozzles to be configured in an open-loop manner that provides independent control without significant flight control interference. Nozzle performance was measured using strain gages installed on the engine mounts to provide a direct in-flight measurement of installed thrust and vectoring forces.[9] Nozzle flap internal and external static pressures were also measured.

The ACTIVE direct thrust measurement method provides measurement of 3-axis thrust forces during axial and vectoring nozzle operation. Steady-state nozzle performance results from an altitude of 30,000 ft and a Mach number of 0.9 are reported in this paper to highlight some nozzle performance findings and illustrate the value of this measurement technique. Data reduction and analysis continues to be done on the remainder of the full-envelope nozzle performance data. Use of trade names or names of manufacturers in this document does not constitute an official endorsement of such products or manufacturers, either expressed or implied, by the National Aeronautics and Space Administration.

The F-15 ACTIVE Aircraft

The test aircraft, NASA 837, is a highly modified pre-production Boeing F-15B with dual Pratt & Whitney (P&W) pitch/yaw balanced beam nozzles (P/Y BBN).[10, 11] Figure 1 summarizes the flight test configuration of the aircraft. Formerly used in the STOL (short takeoff and landing) Maneuver Technology Demonstrator program,[3, 4] the aircraft was selected to serve as the research testbed for the ACTIVE program because of the flexibility of its unique quad-redundant, digital, fly-by-wire, flight and propulsion control system.

Pitch/Yaw Balanced Beam Nozzle

The production F100 balanced beam nozzle (BBN) is of axisymmetric convergent-divergent design. The P/Y BBN extends the capabilities of the proven BBN design; the divergent section provides mechanical vectoring of up to 20° in any circumferential direction

Production design P/Y
thrust vectoring nozzles

F100-PW-229
IPE engines
with IDEECs

Canards

F-15E crew
station

Quad digital
flight controllers

Dual-channel nozzle
controllers

Electronic air inlet
controllers

Tri-channel VMS computer
for research control laws

P/Y BBN features
± 20° vector angle, any direction
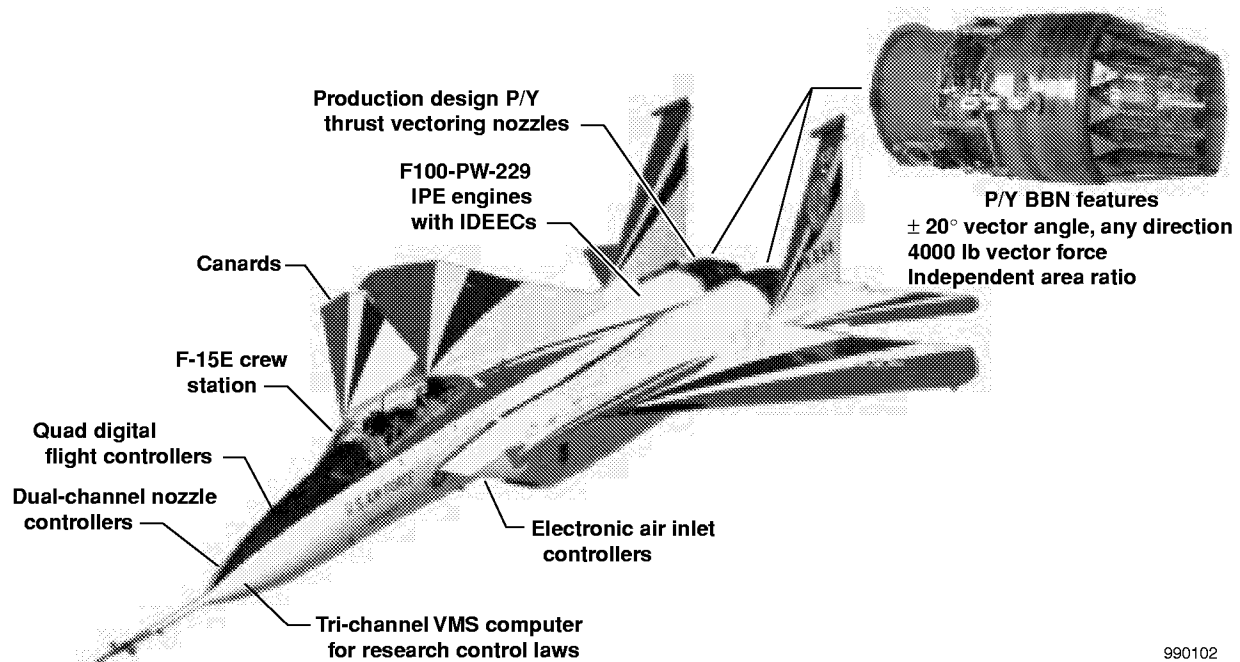4000 lb vector force
Independent area ratio

990102

Figure 1. The ACTIVE vehicle configuration and P/Y BBN design.

(up to a 4,000 lbf maximum vector force limit) and independent nozzle exit-to-throat area ratio modulation capability from 1.1 to 3.[8, 10] The nozzle divergent section is comprised of fifteen flaps which overlay fifteen seals to a varying extent as a function of convergent throat area, area ratio, and vector angle. The divergent section is actuated independently from the convergent section.

Thrust vectoring was accomplished using pre-programmed test inputs to position the nozzle. These inputs were loaded into a research computer prior to flight and were pilot selectable.[11] This open-loop architecture allowed safe, precise and repeatable positioning of the nozzle.

Instrumentation System

Reference 11 gives a description of the ACTIVE instrumentation system. To gain insight into the internal and external flow fields of the nozzle, an array of pressure and temperature sensors were added to the left-hand nozzle. One of the nozzle divergent flaps was instrumented (fig. 2) to measure static pressures, with a total of 6 internal sensors and 1 external sensor. This instrumented flap was located at the 12 o'clock position.

Strain gages were installed on the left engine mounts to measure all 6 force components shown in figure 3. The calibration process consisted of off-aircraft fixture
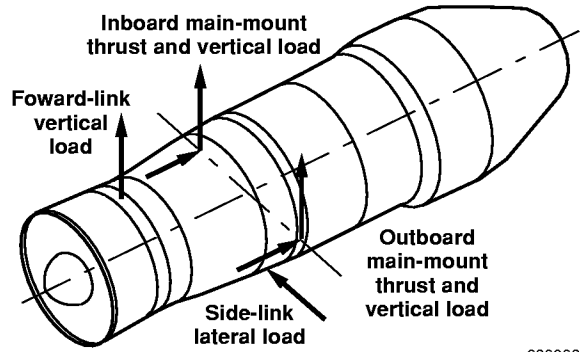

Figure 3. Left engine-mount reactions.

loadings, on-aircraft loadings using dummy engines, off-aircraft heating tests, and a combined systems test conducted on a thrust stand. Each of these calibration steps is described in reference 9, which addressed the measurement of the main mount thrust and the conversion to gross thrust for nonvectored operations. The methodology has been extended to measure vector forces as well as thrust during vectored operations, but space limitations preclude presenting details here.

Assuming that secondary load paths between the engine and airframe are not significant, the thrust and vector forces can be directly determined from the statically determinate reaction equations, after
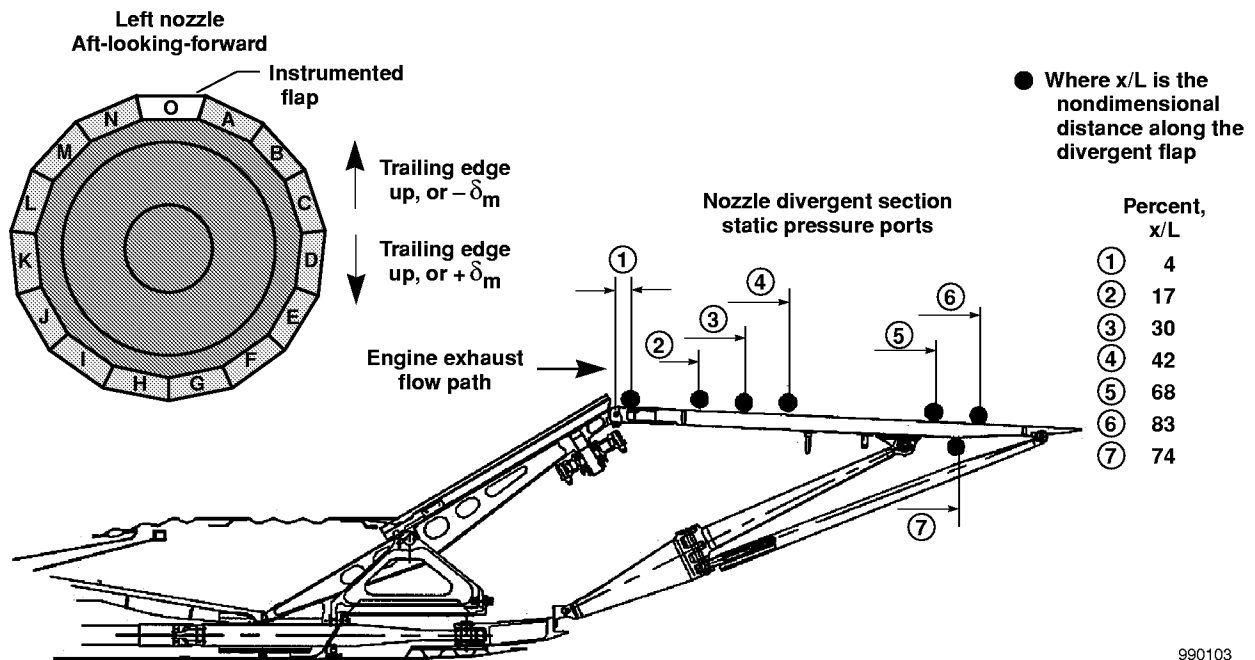
Figure 2. A cross-section of the left nozzle and P/Y BBN indicating static pressure port locations.

correcting for nonengine-generated forces. Because of the flight test techniques and data processing procedures used in the present paper, a relatively simple inertia model provided the only corrections. Gyroscopic force corrections were not required. No corrections for any external nozzle airloads were made, so these components remain an inherent part of the respective thrust and vector forces. Combining uncertainties in the strain gage calibrations, thermal corrections, and inertia model; the total uncertainty level in the extracted thrust and vector forces presented in this paper is estimated to be less than 5 percent.

Flight Test Approach

During open-loop testing, the flight test approach consisted of a coordinated set of aircraft and nozzle configurations, flight conditions, and maneuvers.

Nozzle Configurations

The left-hand nozzle was the primary test nozzle because extensive instrumentation had been installed on it. The right-hand nozzle remained in a nonvectored configuration for data in this report. Nozzle geometric dimensions of throat area, area ratio, and vector angle were varied parametrically. The maximum throat area was 4.2 ft^2, and minimum throat area was 2.9 ft^2. Area ratio, the ratio of nozzle exit area divided by the throat area, varied from a minimum of 1.14 to a maximum of 1.37. The nozzle was vectored to its maximum ±20° limit of pitch or yaw angle. Nozzle pressure ratio, defined as the ratio of nozzle inlet total pressure (pt7) to external ambient pressure (Pamb), ranged from a low of about 3.4 to as high as 5.6 for the data shown in this report. Test inputs were designed to maintain steady vectoring for 5 sec at 2°, 4°, 7°, 10°, and 20° of vector angle.

Flight Conditions and Setup

The Mach 0.9 and altitude of 30,000 ft flight condition served as an *anchor point* where test techniques were developed and data repeatability was verified periodically on different missions. Data and results from this test condition are presented in the Results section of this paper.

Three power settings were employed for this investigation: 43° of throttle (approximate power for level flight), 85° of throttle (maximum non-afterburning power [intermediate power] or military power), and 130° of throttle (maximum afterburning power or maximum power). Prior to commencing data collection the engine was allowed to stabilize thermally and

achieve steady-state thrust levels. During data collection engine throttle position remained fixed.

Test setup involved establishing a 1-*g* wings-level cruise at specified Mach number, altitude, and power setting conditions and when necessary manipulating the right engine throttle to maintain steady-state flight conditions. At maximum power setting it was impossible to establish exactly steady-state conditions of Mach number and altitude because of additional excess thrust. Thus, a quasi-steady-state wings-level climb profile was established. For the maximum power, testing tolerances of ±.05 Mach number and ±2000 ft altitude were created. These tolerance band specifications were derived from sensitivity analysis conducted with a combination of analytical models and flight data so that vector force was not expected to vary more than ±100 lbf over the duration of data collection. Only after the initial setup were vectoring tests accomplished. Vector forces were counteracted by aerodynamic controls and the aircraft remained trimmed in either straight and level flight or the initial climb profile.

Data Reduction Process

Certain aircraft sensors, such as pressure transducers and engine mount strain gages, required corrections to remove known biases. Strain gage-derived thrust force required engine-off tare readings to be removed as a bias correction; whereas bias corrections for the strain gage-derived vector force were applied for each test maneuver.[12] Only results for pitch vector force, (F_p) are reported on and discussed in this report.

Approximately 1.25 seconds (100 samples of data) were used for most test points; mean values were used in all computations. Aircraft normal load factor and nozzle divergent actuator position were analyzed to verify quasi-steady-state conditions had been reached. Data reduction equations were applied to the steady-state data to obtain parameters for strain gage-derived axial and vector forces, and vector force angle.

Propulsive Force Determination

A direct thrust-measurement technique of obtaining modified gross thrust (F_g*) from the engine mount loads was initially developed for quasi-steady-state aircraft and engine operation with a nonvectored nozzle.[9] To minimize the use of uncertain models in determining the measured thrust force from the engine, modified gross thrust (F_g*) was used instead of gross thrust (F_g). For this report, the term "modified gross thrust" includes the nozzle external aerodynamic forces.[13] Because of the lack of a validated model or independent

measurement of only nozzle drag, separation of nozzle drag from the measured $F_g{}^*$ was deemed imprudent. Moreover, from the perspective of designing an integrated flight control that includes thrust vectoring, $F_g{}^*$ may be of more value than F_g.

Secondary load paths such as engine-face inlet seal, airframe-to-nozzle fairings, and engine-bleed ducts may influence thrust and vector force measurement. Results from the installed thrust stand test indicated that secondary load paths were minimal.[9] At the altitude of 30,000 ft and Mach 0.9, it was shown that $F_g{}^*$ of this technique agreed to within 4 percent of an estimated high-fidelity post-flight engine simulation of $F_g{}^*$ (the PW gas generator model of the F100-PW-229[14]). These results for nonvectored operation provided confidence that the technique could be modified to determine both the axial and normal gross thrust components during vectored nozzle operation.

Data collected from calibration testing was used to create an empirical correction for apparent thrust load resulting from vector. The axial component of modified gross thrust ($F_{g_x}{}^*$) during vectoring is determined by summing modified gross thrust, (assuming no vectoring from the direct thrust-measurement technique)[9] with the correction for vectoring. Similarly, the vector force was determined from the strain gage measurements (fig. 3) using appropriate calibrations and corrections. To calculate modified resultant gross thrust during pitch vectoring ($F_R{}^*$) the modified axial gross thrust and pitch vector force (F_p) are combined as a root-sum-square. Further details of this technique are planned to be reported at a later date.

The P&W in-flight engine simulation[14] was used to compute resultant gross thrust (F_R) and served as a benchmark for the direct thrust-measurement technique during vectored operation. Flight measurements such as fuel flows, and flight conditions, were input to the simulation to produce estimates of engine states and performance. For nonvectored operations, the simulation uncertainty of the gross thrust calculation[13] is estimated to be between 2 and 4 percent depending on flight condition and power settings near or above military power; the uncertainty is larger at lower power settings. However, the uncertainty band for the gross thrust calculation is unknown when vectoring is added. Within the engine simulation, the model assumes that the engine exhaust flow is parallel with the nozzle walls. This basic assumption was verified to be reasonable with limited two-dimensional Euler analysis and cold-jet sub-scale wind tunnel testing,[13, 15] but does not match flight test data.[12] Additionally the engine simulation makes no attempt to model external aerodynamic forces such as nozzle lift and drag. Recognizing the modeling limitations, a comparison of the percent difference of F_R for the engine simulation and $F_R{}^*$ of the direct thrust-measurement technique will qualitatively give an assessment of the direct thrust-measurement technique as modified for vectoring operations.

Additional Calculated Parameters

Nozzle performance will be characterized by flow turning efficiency, thrust efficiency, and static pressure distributions of the nozzle divergent section. The vector force angle (δ_f) is determined by the strain gage-based axial and vector loads as follows:

$$\delta_f = \tan^{-1}(F_p/F_{g_x}{}^*)$$

The flow turning efficiency parameter, (δ_f/δ_m) indicates how effectively the nozzle deflects the exhaust plume relative to the nozzle kinematic or mechanical angle, (δ_m). In addition, δ_f includes the forces induced on the nozzle by the external flow. An analysis determined that uncertainty values within 95 percent confidence intervals of δ_f/δ_m range from as high as 40 percent for power for level flight and $2°$ δ_m to as low as 2 percent for maximum power and $20°$ δ_m. Uncertainty levels were a strong function of power setting and vector angle, and decreased with increasing thrust and vector forces.

One measure of thrust efficiency is given by the thrust ratio $F_R{}^*/F_{R0}{}^*$, where $F_{R0}{}^*$ is modified resultant gross thrust at nonvectored conditions. Thrust efficiency relates the total force generation capability of the vectored nozzle relative to a nonvectored nozzle. Ideally, one might expect $F_R{}^*$ to remain constant with δ_m. Variations represent effects such as geometry positioning tolerances, and external and internal flow fields. Additionally, secondary load paths may influence the strain gage force measurements, but as previously noted this is not considered likely. Analysis showed that the uncertainty of the thrust efficiency was a function of power setting and ranged from 1.3 percent at maximum power to 4 percent at power for level flight.

Presentation of Results

Nozzle performance results are presented for testing conducted at power for level flight, military power, and maximum power at a speed of Mach 0.9 and an altitude of 30,000 ft. Flow turning results indicate the nozzle ability to vector engine exhaust and redirect momentum. Thrust efficiency reveals the overall force ($F_{g_x}{}^*$ and F_p)

5

generation potential of the engine and nozzle while vectoring relative to F_R^*. Finally, static pressure distributions lend insight into the internal and external flow characteristics.

Validation of the Direct Thrust Measurement Technique While Vectoring

Figure 4 shows the percent of difference between resultant gross thrust computed from the direct thrust-measurement technique and from the engine simulation at an altitude of 30,000 ft and a Mach number of 0.9. The difference is plotted as a function of vector metal angle for 3 separate power settings: power for level flight, military power, and maximum power.
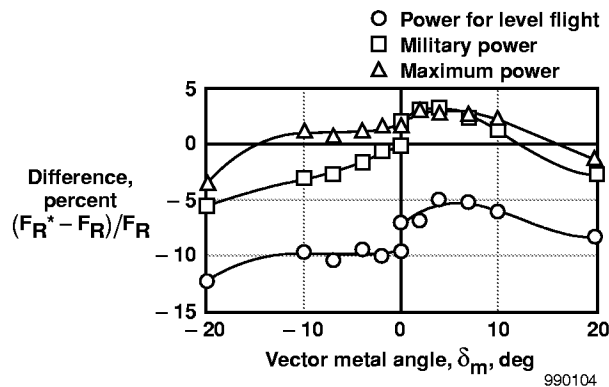
Figure 4. Percent of difference in resultant gross thrust between direct thrust-measurement technique and engine simulation at an altitude of 30,000 ft and Mach 0.9.

The percent differences range from 3 to –12 percent, depending on power setting and vector metal angle. As expected, agreement with the engine simulation is best at maximum power and is worst at the lowest power setting, power for level flight. Slight differences in test conditions give rise to differences seen for each power setting at $0°\delta_m$. For a given power setting, the difference is not a strong function of nozzle vector angle. However, there are asymmetries in the difference evident across the range of δ_m. Differences between the engine simulation and the strain gage direct thrust measurement technique may possibly be attributed to the following causes:

1. Inaccuracies of the simplistic modeling of internal gas path properties such as nozzle discharge coefficient and flow separation during vectoring.

2. Nozzle drag forces which are lumped into the strain gage measurement but not included in the model.

3. The lack of a model to account for nozzle mechanical effects.

4. Thrust measurement uncertainty.

The engine simulation makes no attempt to account for nozzle flow separation in the divergent section and the effect it has on gross thrust. It will be shown in a later section that significant flow separation occurs at some conditions. As the nozzle is vectored, the minimum internal area that defines the nozzle throat and the location in the nozzle where the flow chokes rotates as a function of metal vector angle. Additionally the flow choke point that defines the aerodynamic throat may not always coincide with the minimum mechanical throat area, for reasons not thoroughly understood. The engine simulation makes a simplifying assumption about the rotation of the flow choke point; its movement is directly proportional with the cosine of the vector angle. Furthermore, the model assumes that the nozzle discharge coefficient, which directly affects predicted gross thrust, also varies with the cosine of the vector angle. This assumption has not been verified and opens up the possibility of modeling error. Clearly there are areas where modeling fidelity could be improved based on experimental results.

For a given set of flight conditions and power settings, nozzle drag is expected to vary substantially with vector angle. Nozzle drag forces during vectoring are not known to have ever been measured in flight, but only in limited subscale wind tunnel tests. Nozzle drag is very difficult to analytically determine because of its sensitivity to aircraft and nozzle external geometry and the complex highly viscous flow field about the nozzle and aircraft aft structure. However, for nonvectored nozzles, nozzle drag forces become considerable at certain conditions relative to engine gross thrust.

Postflight examinations of the nozzle provided indications that unanticipated divergent flap and seal positions were experienced at some point during the flight. It is believed that slight seal deflections occur with certain vectoring conditions, which may allow for flow crossing through gaps between flaps and seals. At this point the phenomena is unpredictable and not well understood, but it could affect nozzle propulsive forces.

In summary, all results comparing the strain gage direct thrust-measurement technique and the engine simulation fall within the expected uncertainty bands of each technique. These results provide a validation and a positive qualitative assessment of the direct thrust-measurement technique as modified for vectoring operations, especially at military and maximum power settings.

6

Flow Turning Efficiency Results

Figure 5 presents results for flow turning efficiency. Because of the axisymmetric nozzle design, the results are somewhat symmetric with vector metal angle; peak turning efficiencies occur at the smallest tested δ_m and gradually fall off as δ_m increases. Because of the greater uncertainty of vector force measurements at small δ_m, uncertainty in δ_f/δ_m is greater for smaller δ_m. Flow turning efficiency is inversely proportional to power setting; as power setting rises, lower vector force angles are achieved for a given vector metal angle. Flow overturning, where δ_m/δ_f is greater than 1 is seen at the military and power for level flight settings, but not at maximum power. At most power settings where flow separation is not present, flow overturning is predicted from subscale testing and Euler analysis. Based on these flight test results, the fidelity of these predictions is questionable, especially at higher power settings.

At maximum power, the nozzle is unable to deflect the higher momentum engine exhaust flow as efficiently as it does for lower power settings. Geometric differences in the nozzle divergent section between power settings may explain the flow turning capability of the nozzle. At maximum power the engine passes more airflow and has a larger throat area than at military power or power for level flight. As a result, core exhaust flow at maximum power is relatively less influenced by boundary effects at the nozzle walls. At a power for level flight setting, where the flow has relatively less momentum and the throat is relatively small, flow overturning occurs within $\pm10°$ δ_m. Beyond $10°$ δ_m, flow turning losses associated with flow separation, or internal shock wave interference may reduce the nozzle effectiveness. External nozzle forces may also affect the readings. The
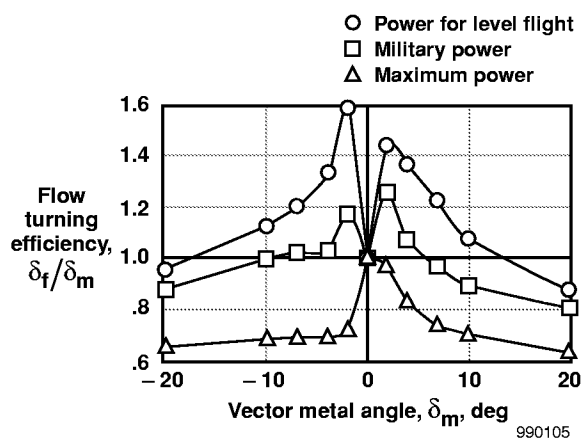
effects of reduced flow turning efficiency at maximum power is partially offset by the fact that absolute vector force remains high, so that even with reduced vector force angles the high thrust levels associated with maximum power produce high vector forces.

Thrust Efficiency Results

Figure 6 shows thrust efficiency, F_R^*/F_{R0}^* plotted against δ_m. Results indicate that the total force generated by the nozzle remains high for all power settings and vector angles, particularly for positive δ_m. By definition, the thrust efficiency is 100 percent at a $0°$ δ_m. The lack of symmetry in thrust efficiency relative to δ_m reflects the combined effects of nozzle hardware asymmetries and asymmetric flow patterns. As the nozzle is vectored, it encounters varying levels of force exerted by the internal and external flow. External force asymmetries arise because of differences in the flow patterns beneath and above the nozzle near the aft end of the aircraft. Small nonmeasurable deflections in the nozzle divergent section can occur depending on the pressure levels. These small changes in geometry, in turn, affect the internal flowpath that the exhaust must pass through and the momentum that transfers to the nozzle. Another potential contributor to thrust efficiency asymmetries may be interference effects as previously discussed. Secondary load paths may occur differently depending on whether the engine is responding to positive or negative vectoring forces. The most likely significant candidate for a secondary load path is at the inlet seal. Position transducer instrumentation at the front of the engine near the inlet seal did not reveal evidence of inlet seal interference. If secondary load paths exist, the effect would be to reduce the measurable forces.
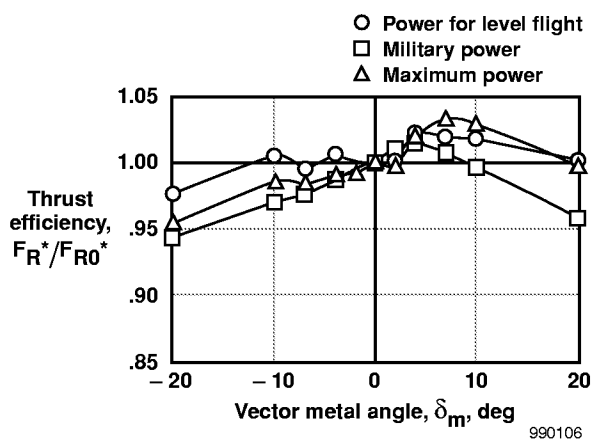

Figure 5. Flow turning efficiency at Mach 0.9 and an altitude of 30,000 ft.

Figure 6. Thrust efficiency at Mach 0.9 and an altitude of 30,000 ft.

7

Initially, thrust efficiency was expected to be greatest for a nonvectored nozzle because of nozzle geometric symmetry and the predicted losses associated with redirecting a highly energized exhaust flow. However, contributions from external aerodynamic forces on the nozzle can positively benefit the nozzle by increasing the amount of measurable propulsive force. Vectoring may also improve internal nozzle efficiency. An overall peak efficiency of 103.5 percent occurs at maximum power near 7° δ_m. Thrust efficiencies greater than 100 percent are significant in that the additional propulsive force lends itself to greater overall vehicle efficiencies. Efficiencies greater than 100 percent could also have a substantial impact on design tools and simulations. In the negative or trailing edge up direction, efficiency declines except at power for level flight where efficiency remains relatively flat. As previously noted, however, uncertainty of the results is greatest at the power for level flight setting. Overall, efficiencies never fall below 95 percent.
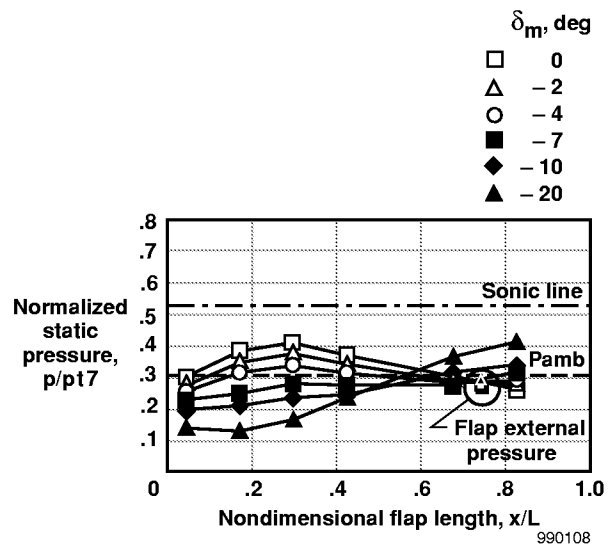
Static Pressure Distribution Results

Figures 7 to 9 show static pressure distributions, normalized to $pt7$. The pressure ratios are plotted against nondimensional distance along the flap, x/L for δ_m of 20°, 10°, 7°, 4°, 2°, and 0° or nonvectored. Curves for each δ_m connect data points from each internal static pressure port but are not meant to imply data were collected between the data points; external port data points are highlighted. For additional reference, the figure shows Pamb as measured from an aircraft mounted noseboom and the sonic line as determined from 1-dimensional isentropic gas dynamics.

Consistent results were obtained at all power settings for the nonvectored nozzle; the nozzle was full-flowing, exhausting near local ambient external pressure, and there were no signs of shocks or separation.

When vectored, the nozzle has significantly different flow characteristics than the nonvectored nozzle. As shown in figures 7(a), 8(a), and 9(a), pressures along the flap during positive vectoring experience substantial rises in pressure that are above the nonvectored case. For negative vectoring angles, the pressures along the flap experience varying degrees of a static pressure rise as seen in figures 7(b), 8(b), and 9(b). An example of this is shown in figure 7(b) for power for level flight. At 7° δ_m, the pressure rises predominantly at 70- to 80-percent down the flap. As the nozzle is further vectored, the area of pressure rise is most pronounced at 20° δ_m. As power setting rises, the area of static pressure rise declines.
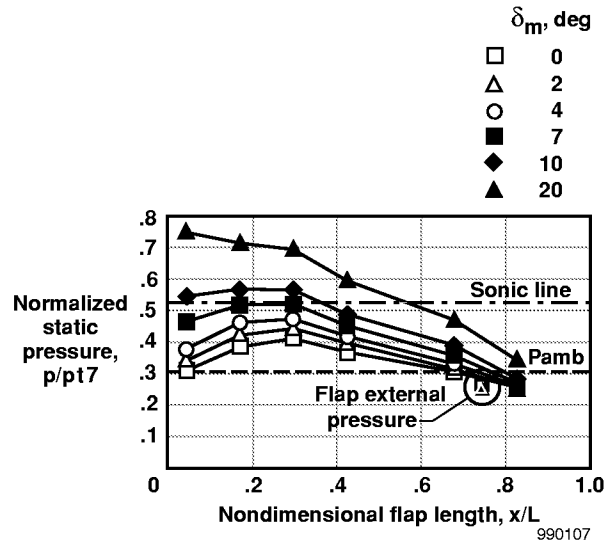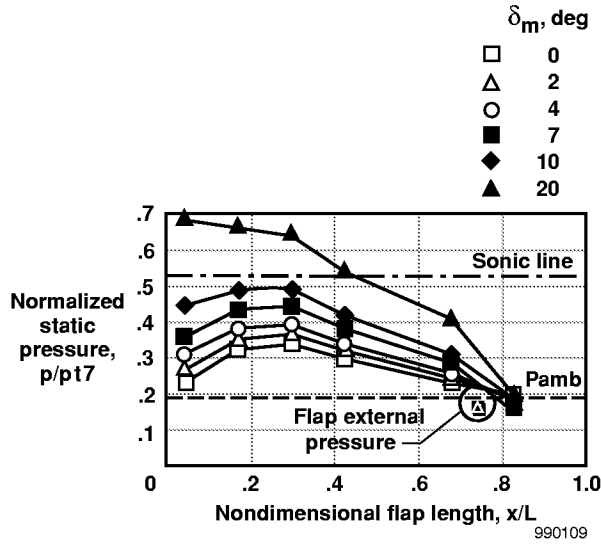

(a) Positive δ_m.
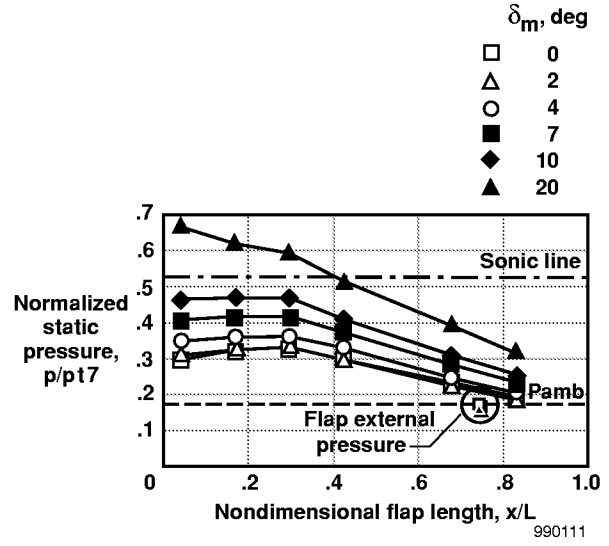

(b) Negative δ_m.

Figure 7. Static pressure distribution for power for level flight.

The pressure distributions also indicate that the actual nozzle throat for the vectored nozzle is inclined. For 20° δ_m, the aerodynamic throat (indicated on the figures by the sonic line where $p/pt7 = 0.528$) occurs at $x/L \approx .55$ for power for level flight, at $x/L \approx .45$ for military power, and at $x/L \approx .40$ for maximum power. As the power level rises, the throat has rotated forward down the flap. Because of this inclined throat, much of the flow turning is accomplished at subsonic conditions,
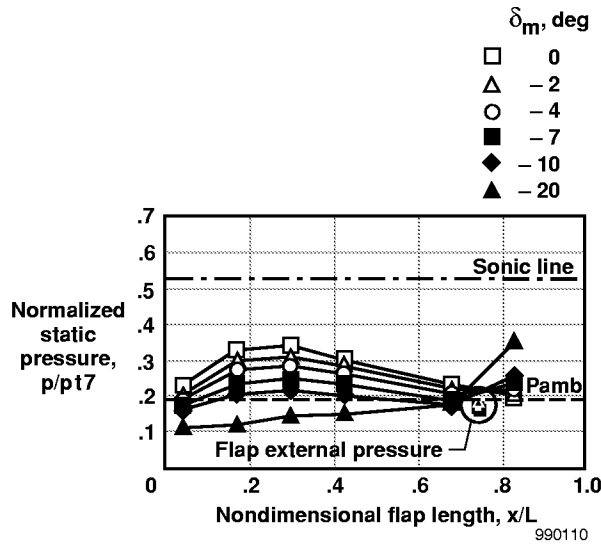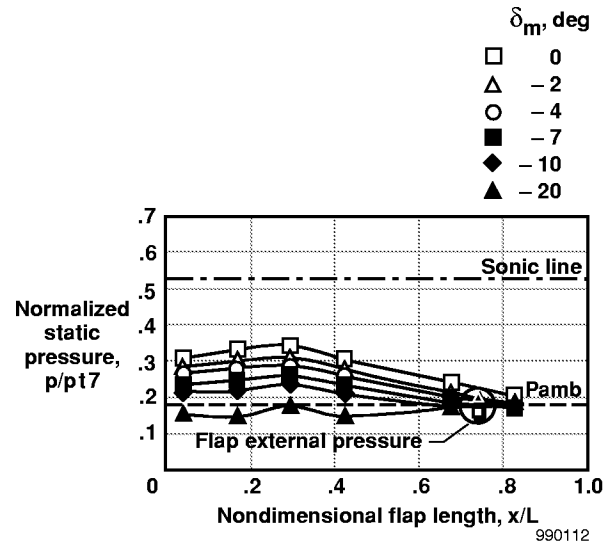
8

(a) Positive δ_m.

(a) Positive δ_m.

(b) Negative δ_m.

(b) Negative δ_m.

Figure 8. Static pressure distribution for military power.

Figure 9 Static pressure distribution for maximum power.

which diminishes flow turning losses. Larger flow turning losses occur with supersonic rather than subsonic flow turning.[16] The larger area of efficient subsonic flow turning at power for level flight as compared to the other power settings supports the flow turning results shown in figure 5.

With the single external pressure measurement, there are very few signs of external flow response to vectoring. Caution is given that this is a limited result

taken at one location along the top flap, obtained at Mach 0.9 and an altitude of 30,000 ft for pitch vectoring, and should not be extended beyond these conditions. However, data recorded at other flight conditions and nozzle configurations have been collected and are currently being reduced; some of which indicate external flow field sensitivity to pitch vectoring. More comprehensive results of external pressure measurements at other flight conditions are planned to be reported at a later date.

Concluding Remarks

The F-15 ACTIVE nozzle performance flight test experiment has successfully measured the flow turning and thrust efficiency capability of a hydromechanically vectored axisymmetric thrust-vectoring nozzle. A technique whereby strain gages installed onto engine mounts provided for the direct measurement of thrust and vector forces has proven to be extremely valuable for the in-flight assessment of thrust-vectoring nozzle performance. Internal and external nozzle static pressure distributions were also measured in-flight and provided unique insight into the flow fields of the vectoring nozzle.

Flight research has led to the following major findings for results obtained at an altitude of 30,000 ft and a speed of Mach 0.9:

- Flow turning efficiency varied significantly from predictions.

- Vector force angles did not closely track geometric vector angle.

- Thrust efficiency levels at some vectored configurations were greater than nonvectored.

- The strain gage method of in-flight extraction of propulsion forces was verified.

Flight test results disagree with subscale wind tunnel testing and inviscid computational fluid dynamic analysis that predicted vast regions of flow overturning, where the exhaust flow is deflected beyond the nozzle geometric vector angle. Flight test measurements indicate flow overturning was limited to the low power settings and vector angles. However, at maximum power, considerable flow underturning was observed, and flow turning efficiency was degraded compared to the low power settings. Therefore, it is recommended that additional flight test or analysis be conducted to understand errors from subscale wind tunnel testing and computational analysis.

Results of pitch vectoring tests at an altitude of 30,000 ft and a speed of Mach 0.9 demonstrated that flow turning and thrust efficiency varied substantially with power setting and vector angle. Flow turning was greatest at low power settings, and thrust efficiency was greatest at the highest power setting. Despite a symmetric nozzle design, thrust efficiency results were unexpectedly found to be asymmetric. The influence of external aerodynamic nozzle forces and localized nozzle geometry asymmetries during vectoring are the likely causes. Even with the inherent losses associated with redirecting a highly energized exhaust flow, peak thrust efficiency occurred in a trailing edge down vectored configuration. Contributions from external aerodynamic nozzle forces overcome turning losses and positively benefit the nozzle by increasing the amount of measurable propulsive force. The possibilities of harnessing the additional propulsive force provided by vectoring are numerous.

Internal static pressure distributions indicated large regions of subsonic flow turning, especially at the lowest power setting, and substantiated the independent flow turning findings that were based on the strain gage method. Additionally, the static pressure rise became more widespread along the nozzle wall as power settings decreased and vector angle increased. The relatively smaller area of separation seen at maximum power also confirms the thrust efficiency results.

The direct thrust and vector force measurement technique showed good agreement with a high-fidelity engine simulation, even during vectoring. This novel approach provides a direct method to measure vector flow turning efficiency and thrust efficiency. This technique inherently includes nozzle aerodynamic loads and thus provides a complete overall assessment of nozzle performance effects on the vehicle during vectoring. Differences found between the direct measured forces and the model may be attributed to inaccurate modeling of the aerodynamic loads, exhaust flow characteristics, nozzle hardware particulars, and thrust measurement uncertainty. In summary, all results comparing the strain gage measurements to the engine model agree within the expected uncertainty bands of each technique. This provides confidence in the performance results presented in this report. The results presented in this paper illustrate the value of flight test to vehicle performance integration issues that are difficult to model or duplicate in the laboratory.

References

[1]Regenie, Victoria, Donald Gatlin, Robert Kempel, and Neil Matheny, *The F-18 High Alpha Research Vehicle: A High-Angle-of-Attack Testbed Aircraft*, NASA TM-104253, Sept. 1992.

[2]Canter, Dave, "X-31 Post-Stall Envelope Expansion and Tactical Utility Testing," *Fourth NASA High Alpha Conference*, NASA CP-10143, vol. 2, July 1994.

[3]Crawford, Mark, Brian Hobbs, Steven Roell, and Gerard Schkolnik, *STOL/Maneuver Technology Demonstrator Flying Qualities and Integrated*

Flight/Propulsion Control System Evaluation, Final Report, AFFTC-TR-91-29, Dec. 1991.

[4]Crawford, Mark and Michael J. Costigan, *STOL/ Maneuver Technology Demonstrator Performance and Propulsion System Evaluation, Final Report,* AFFTC-TR-91-30, Dec. 1991.

[5]Kidman, David S., Jesse E. Vickers, Brian P. Olson, and Michael A. Gerzanics, *Evaluation of the F-16 Multi-Axis Thrust Vectoring Aircraft,* AFFTC-TR-95-12, Sept. 1995.

[6]Bowers, Albion H. and Joseph W. Pahle, *Thrust Vectoring on the NASA F-18 High Alpha Research Vehicle,* NASA TM-4771, Nov. 1996.

[7]Johnson, Steven A., *Aircraft Ground Test and Subscale Model Results of Axial Thrust Loss Caused By Thrust Vectoring Using Turning Vanes,* NASA TM-4341, Jan. 1992.

[8]Berger, C.W. and C. B. Wood, "Pratt and Whitney's Multi Axis Thrust Vectoring Engine Exhaust Nozzle Design, Development, Flight Test Techniques, and Results," to be published in the *Proceedings of the 14th International Society for Air Breathing Engines* (ISOABE), Sept. 1999.

[9]Conners, Timothy R. and Robert L. Sims, *Full Flight Envelope Direct Thrust Measurement on a Supersonic Aircraft,* AIAA-98-3872, July 1998.

[10]Doane, P., R. Bursey, and G. Schkolnik, *F-15 ACTIVE: A Flexible Propulsion Integration Testbed,* AIAA 94-3360, June 1994.

[11]Smolka, James W., Laurence A. Walker, Gregory H. Johnson, Gregory S. Schkolnik, Curtis W. Berger, Timothy R. Conners, John S. Orme, Karla S. Shy, and C. Bruce Wood, "F-15 ACTIVE Flight Research Program," *1996 Reports to the Aerospace Profession: Fortieth Symposium Proceedings,* Society Of Experimental Test Pilots, Sept. 1996, pp. 112–145.

[12]Orme, John S., Ross Hathaway, and Michael D. Ferguson, *Initial Flight Test Evaluation of the F-15 ACTIVE Axisymmetric Vectoring Nozzle Performance,* NASA TM-206558, July 1998.

[13]Society of Automotive Engineers, Incorporated, Committee E-33, U*ncertainty of In-Flight Thrust Determination,* SAE-AIR-1678, Aug. 1985.

[14]*F100-PW-229 Status Simulation With P/Y BBN Vectoring Capability, User's Manual for Customer Computer Deck CCD 1430-00.0,* Pratt & Whitney Co., West Palm Beach, Florida, FR-20248, Dec. 1994.

[15]Wing, David J. and Francis J. Capone, *Performance Characteristics of Two Multiaxis Thrust-Vectoring Nozzles at Mach Numbers up to 1.28,* NASA TP-3313, May 1993.

[16]Carson, George T., Jr. and Francis J. Capone, *Static Internal Performance of an Axisymmetric Nozzle With Multiaxis Thrust-Vectoring Capability,* NASA TM-4237, Feb. 1991.

REPORT DOCUMENTATION PAGE

Public reporting burden for this collection of information is estimated to average 1 hour per response, including the time for reviewing instructions, searching existing data sources, gathering and maintaining the data needed, and completing and reviewing the collection of information. Send comments regarding this burden estimate or any other aspect of this collection of information, including suggestions for reducing this burden, to Washington Headquarters Services, Directorate for Information Operations and Reports, 1215 Jefferson Davis Highway, Suite 1204, Arlington, VA 22202-4302, and to the Office of Management and Budget, Paperwork Reduction Project (0704-0188), Washington, DC 20503.

1. AGENCY USE ONLY (Leave blank)	2. REPORT DATE	3. REPORT TYPE AND DATES COVERED
	September 1999	Conference Paper

4. TITLE AND SUBTITLE

Selected Performance Measurements of the F-15 ACTIVE Axisymmetric Thrust-Vectoring Nozzle

6. AUTHOR(S)

John S. Orme and Robert L. Sims

5. FUNDING NUMBERS

WU 529-20-24-00-33-00-MGT

7. PERFORMING ORGANIZATION NAME(S) AND ADDRESS(ES)

NASA Dryden Flight Research Center
P.O. Box 273
Edwards, California 93523-0273

8. PERFORMING ORGANIZATION REPORT NUMBER

H-2339

9. SPONSORING/MONITORING AGENCY NAME(S) AND ADDRESS(ES)

National Aeronautics and Space Administration
Washington, DC 20546-0001

10. SPONSORING/MONITORING AGENCY REPORT NUMBER

H-2339

11. SUPPLEMENTARY NOTES

12a. DISTRIBUTION/AVAILABILITY STATEMENT

Unclassified—Unlimited
Subject Category 05 and 07

12b. DISTRIBUTION CODE

13. ABSTRACT (Maximum 200 words)

Flight tests recently completed at the NASA Dryden Flight Research Center evaluated performance of a hydromechanically vectored axisymmetric nozzle onboard the F-15 ACTIVE. A flight-test technique whereby strain gages installed onto engine mounts provided for the direct measurement of thrust and vector forces has proven to be extremely valuable. Flow turning and thrust efficiency, as well as nozzle static pressure distributions were measured and analyzed. This report presents results from testing at an altitude of 30,000 ft and a speed of Mach 0.9. Flow turning and thrust efficiency were found to be significantly different than predicted, and moreover, varied substantially with power setting and pitch vector angle. Results of an in-flight comparison of the direct thrust measurement technique and an engine simulation fell within the expected uncertainty bands. Overall nozzle performance at this flight condition demonstrated the F100-PW-229 thrust-vectoring nozzles to be highly capable and efficient.

14. SUBJECT TERMS

Axisymmetric nozzle, Direct thrust measurement, F-15 ACTIVE, Flight tests, Nozzle aerodynamic loads, Nozzle drag, Nozzle flow field, Nozzle performance, Thrust efficiency, Thrust measurement, Thrust vectoring

15. NUMBER OF PAGES

12

16. PRICE CODE

A03

17. SECURITY CLASSIFICATION OF REPORT	18. SECURITY CLASSIFICATION OF THIS PAGE	19. SECURITY CLASSIFICATION OF ABSTRACT	20. LIMITATION OF ABSTRACT
Unclassified	Unclassified	Unclassified	Unlimited